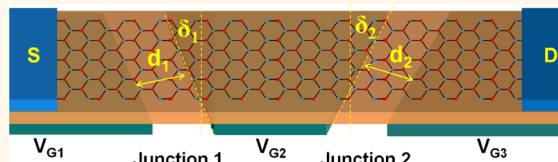# Manipulating Chiral Transmission by Gate Geometry: Switching in Graphene with Transmission Gaps

Redwan N. Sajjad* and Avik W. Ghosh*

Department of Electrical and Computer Engineering, University of Virginia, Charlottesville, Virginia 22904, United States

**ABSTRACT** We explore the chiral transmission of electrons across graphene heterojunctions for electronic switching using gate geometry alone. A sequence of gates is used to collimate and orthogonalize the chiral transmission lobes across multiple junctions, resulting in negligible overall current. The resistance of the device is enhanced by several orders of magnitude by biasing the gates into the bipolar *npn* doping regime, even as the ON state in the homogeneous *nnn* regime remains highly conductive. The mobility is preserved because the switching involves the suppression of transmission over a range of energy (transmission gap) instead of a structural band gap that would reduce the number of available channels of conduction. Under a different biasing scheme (npn to npp), this transmission gap can be made highly gate tunable, allowing a subthermal turn-on that beats the Landauer bound on switching energy, limiting present-day digital electronics.

**KEYWORDS:** graphene · chiral transmission · gate geometry · transmission gap · Landauer limit · heterojunctions

The intriguing possibilities of graphene derive from its exceptional electronic[1−5] and material properties,[6−8] in particular, its photon-like band structure,[9] negative refractive index electron "optics",[10−12] ultrahigh mobility,[13,14] pseudospin physics,[15] and improved 2-D electrostatics.[16] Its switching ability, however, is compromised by the lack of a band gap,[17] while opening a gap structurally eliminates the available modes for conduction, degrading mobility.[17,18] This begs the question as to whether we can significantly modulate the conductivity of graphene without any structural distortion, thereby preserving its superior mobility. A way to do this is to open a transmission gap that suppresses the transmission, without actually shutting off the density of states. The dual attributes that help graphene electrons achieve such goal as we show in this paper are its photon-like trajectories[10] and chiral nature.[19] These make the device resistance dependent upon the physical parameters of the gates, such as orientation and relative position.

In an earlier paper,[20] we outlined how we can open a transmission gap by a tunnel barrier, by angularly injecting the electrons with a quantum point contact (QPC) and then selectively eliminating the low incidence angle Klein tunneling[21,22] modes with a barrier,

in that case a patterned antidot or an insulating molecular chain. When the critical angle for total internal reflection is lower than the angle subtended at the QPC by the barrier, electrons are unable to cross over across the junction. The result is a transmission gap that can be collapsed by driving the voltage gradient across the junction toward the homogeneous pp or nn limit, creating a subthermal turn-on sharper than the Landauer binary switching limit of $kT\ln2$ for distinguishability ($kT\ln10$ for each decade rise in current). Beyond proof of concept, that geometry was limited by a paucity of QPC modes and the structural distortions near the barrier that create a larger effective footprint.

In this paper, we combine a split gated pn junction to collimate the transverse modes (Figure 1a), with recently demonstrated[23,24] action of a tilted pn junction that increases the effective angle of incidence of the electrons. The conductance at zero temperature can be written as

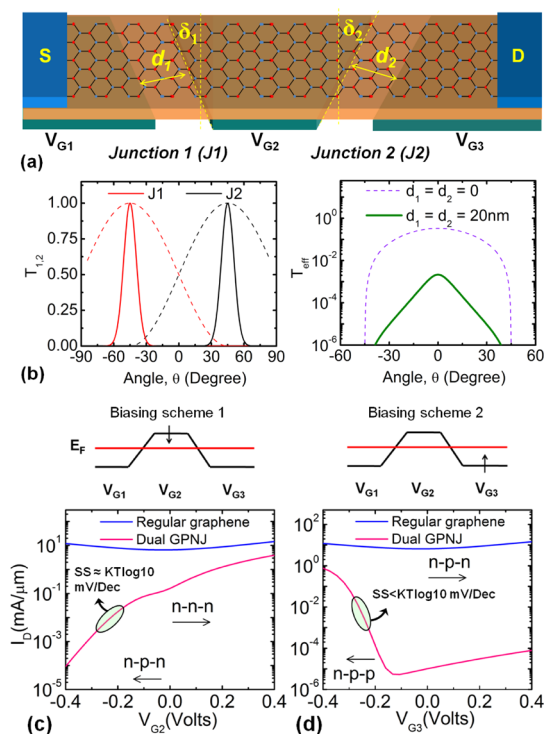$$G(E_F) = G_0 \sum_{n=1}^{M(E_F)} T_n = G_0 M T_{av} \qquad (1)$$

where $G_0 = 4q^2/h$ is the conductance quantum which includes spin and valley degeneracy, $M$ is the total number of transverse modes, $T_n$ is transmission of individual modes. If all modes transmit with equal probability ($T$),

**Figure 1.** (a) Chiral tunneling in graphene pn junction (GPNJ) manipulated with gate geometry, using two junctions (dual GPNJ) tilted in opposite directions, (b) making their angle-dependent transmission lobes orthogonal (left) and yielding negligible overall transmission (right) for split gates (solid line). (c) Transmission gap creates a high ON−OFF current ratio as a function of $V_{G2}$ at finite bias, $V_{DS} = 0.4$ V and room temperature. The ON current degrades slightly compared to homogeneous gapless graphene, but the OFF current is reduced by several orders of magnitude. (d) Steeper change (beating $KT\ln 10$ switching limit) of current with $V_{G3}$. This is done by keeping the collimation effect of the first junction intact and making the transmission gap dependent upon Snell's law. Transport formalism is accomplished for 2D bulk graphene and edge reflections are ignored.

the conductance can simply be written as $G_0 MT$. Due to chiral nature of carriers in graphene, transmission in graphene pn junction (GPNJ) is highly angle (mode)-dependent, making it necessary to work with an average transmission per mode $T_{av}$ over all modes. Instead of eliminating the mode count $M$ as does a structural band gap, we exploit instead the chiral (anisotropic) tunneling that makes $T_{av}$ vanishingly small (Figure 1b) over a range of energies. This results in low OFF current (Figure 1c,d). All modes are available for conduction in the ON state when the split gates are set to the same polarity, thus retaining the high mobility of graphene.

## RESULTS AND DISCUSSION

**Opening the Transmission Gap with Gate Geometry.** Figure 1 shows two pn junctions tilted (at angle $\delta$) in opposite directions. Each junction exploits chiral tunneling that conserves pseudospin index and maximizes transmission for normal incidence (Klein tunneling). Transmission is suppressed for nonzero incidence angles, especially when the potential varies

smoothly, that is, the p to n transition occurs over a finite split gate distance $2d$.[25] A tilted junction rotates the transmission lobe accordingly,[24] shifting transmissions along opposite directions to make them orthogonal. The mode-averaged transmissions across the dual junction can be decomposed as below (see Supporting Information for details).

$$T_{1,2}(\theta) \approx \left[ \frac{\cos(\theta_L \pm \delta)\cos\theta_R}{\cos^2\left(\dfrac{\theta_L \pm \delta + \theta_R}{2}\right)} \right] \quad (2)$$

$$\times \exp\left[-\pi 2d \frac{k_{FL} k_{FR}}{k_{FL} + k_{FR}} \sin(\theta_L \pm \delta)\sin(\theta_R)\right]$$

$$\frac{1}{T_{eff}} \approx \frac{1}{T_1} + \frac{1}{T_2} - 1 \quad (3)$$

$$T_{av}(E_F) = \frac{1}{2}\int T_{eff}(\theta)\cos\theta \, d\theta$$
$$= [A\sqrt{k_F d}\, e^{\pi k_F d \sin^2\delta}]^{-1} \quad (4)$$

$T_{av}$ is vanishingly small for moderate doping. Equation 4 is written for symmetric npn doping with Fermi wavevector, $k_F = E_F/(\hbar v_F)$ and $A \approx 8$ is a constant. The angular representation of a mode is given by $\theta = \tan^{-1} k_y/k_x$, where $k_y$ and $k_x$ are the transverse and longitudinal components of $k_F$. Equation 2 arises from matching pseudospins across the junction, L and R denoting components to left and right of a junction (1,2).[26] The tilt $\delta$ modifies the incident angle by $\theta_L \pm \delta$, and the angle of refraction is related to incident angle through Snell's law, $k_{FL}\sin(\theta_L \pm \delta) = k_{FR}\sin\theta_R$. Equation 3 assumes resistive addition of the junction resistances and ballistic flow in between. The mode count for width $W$ is given by $M = (Wk_F)/\pi$. The resulting total conductance $G_0 MT_{av}$ is negligible in the entire pn junction regime, indicating that the transmission gap ($E_G$) exists if the carrier densities have opposite polarities

$$E_G \approx V_0 \quad (5)$$

where $V_0$ is the gate-induced potential step across the junction. This is because the high resistance is primarily contributed by the WKB exponential factor which is present in the pn regime, whereas the unipolar regime has only the cosine prefactors representing the wave function mismatch.[26,27] Significantly, eq 2 predicts two critical angles for total internal reflection: a Snell's-law-driven $\theta_C = \sin^{-1}(n_R/n_L)$ arising from the prefactor and a second smaller $\theta_C \sim 1/(\pi k_F d)^{1/2}$ from the WKB term.

Figure 2 shows variation of $T_{av}$ numerically calculated from eq 2 as a function of Fermi energy ($E_F$) for four different devices and doping profiles. The orange line shows unit transmission of all modes for a ballistic uniformly doped graphene sheet. The angular (mode-dependent) transmission is manifested in a single sharp ($d = 0$) graphene pn junction, and the $T_{av}$ is suppressed (blue dash). Further suppression is achieved with a split junction (pink circles) (nonzero $d$) due to high transverse
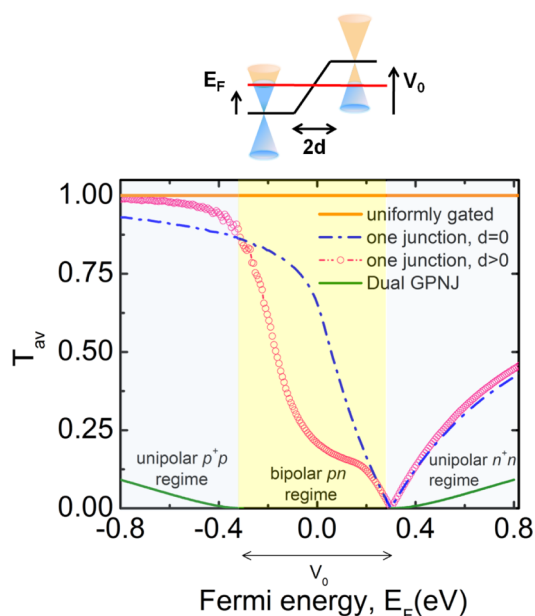
**Figure 2.** Mode-averaged transmission $T_{av}$ vs Fermi energy $E_F$ for different doping profiles (Fermi energy $E_F$ and built-in potential $V_0$ are indicated on the top band diagram). $T_{av}$ for the dual tilt GPNJ shows a gap (green line), which is termed as transmission gap (yellow shading) in this paper.

energy (mode) filtering. $T_{av}$ for the device in Figure 1a is shown in green, showing a negligible transmission over the bipolar doping regime. Note that both green and pink lines show suppression only in the bipolar doping regime, outside which the exponential scaling in eq 2 is eliminated.[26]

The minimum current is achieved in the npn regime (OFF state). Over the energy window $[\mu_S, \mu_D] = [E_F, E_F - qV_{DS}]$ set by the drain voltage $V_{DS}$, $T_{av}$ varies weakly, so that the OFF state current at zero temperature for the npn configuration can be extracted from

$$I_{OFF} = G_0 \int_{\mu_D}^{\mu_S} M(E) T_{av}(E) dE \qquad (6)$$
$$\approx G_0 M(E_F) T_{av}(E_F) V_{DS}$$

convolved with the thermal broadening function for finite temperature. For uniformly doped graphene with ballistic transport

$$I_{ON} = G_0 M(E_F) V_{DS} \qquad (7)$$

so that the zero temperature ON−OFF ratio simply becomes

$$I_{ON}/I_{OFF} \approx [T_{av}(E_F)]^{-1} \sim A \sqrt{k_F d}(2e^{\pi k_F d \sin^2 \delta}) \qquad (8)$$

if the biasing is changed all the way from npn to nnn. Figure 1c (pink line) shows the change in dual tilt GPNJ current with gate voltage $V_{G2}$ at room temperature and finite drain bias ($V_{DS}$), compared with a regular zero band gap graphene-based device (blue line). From the nin to nnn regime, we see little change in GPNJ current on a log scale, but toward the npn regime, we see at least 3 orders of magnitude decrease when the Fermi
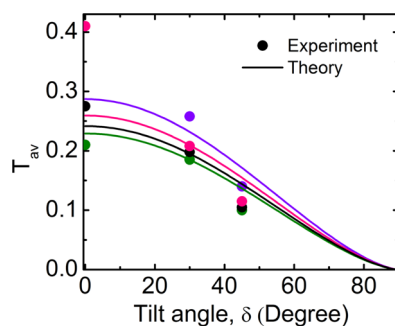


**Figure 3.** Benchmarking $T_{av}$ with experiment[23] for a single tilted split junction for several gate voltages. Experiment shows good agreement with the theory, confirming the angular shift of $T(\theta)$ and the scaling law with tilt.

window remains mostly within the transmission gap. Compared to the blue line, the ON current is reduced only slightly, while the OFF current is reduced by several orders of magnitude. The reduction in ON current is due to the fact that the doping is not quite uniform at the ON state across the n⁺n collimator (maintained at unequal doping to avoid a large voltage swing), whereupon the wave function mismatch leads to lower current than usual. Fully ballistic transport and assuming high-quality contact gives us an intrinsic ON current in the mA/$\mu$m regime. In this calculation, the gate parameters are $|\delta_1| = |\delta_2| = \delta = 45°$, $d_1 = d_2 = 20$ nm, $V_{G1} = V_{G3} = +1$ V, $V_{DS} = 0.4$ V.

Critical to the geometric switching is the prominance of angle-dependent chiral transmission across a tilted junction. Figure 3 shows the mode-averaged transmission $T_{av}$ extracted (see Methods) from the measured junction resistance for a single split junction, for varying tilt angles.[23] For an abrupt tilted junction, $T_{av} = 2/3 \cos^4(\delta/2)$ in the symmetric pn doping limit and represents an electronic analog of Malus' law—the quenching of light transmission through a polarizer−analyzer pair. The reduction in $T_{av}$ originates from the angular shift of transmission lobe (Figure 1b) in the low angular mode density region.[24] The numerically evaluated $T_{av}$ generalized for a tilted split junction (solid lines) agrees well with experimental data (dots) for different gate voltages. The scaling of $T_{av}$ in experiment thus confirms the angular shift of the transmission lobe and forms the basis of the proposed device. The data show an absence of specular edge scattering and persistence in presence of charge puddles. The detailed theoretical model can be found in ref 24.

**Biasing Scheme and Impact on Subthreshold Slope.** For a semiconductor with fixed band gap, rate of change of current with gate voltage is $kT\ln(10)/q$ and limits the energy dissipation in binary switching. The limit arises from the rate of change in overlap between the band edge and the Fermi−Dirac distribution, normally set by the Boltzmann tail. In our device, transmission gap is sensitive to how gate voltages are varied because it is a gate-voltage-dependent transport gap. There can be
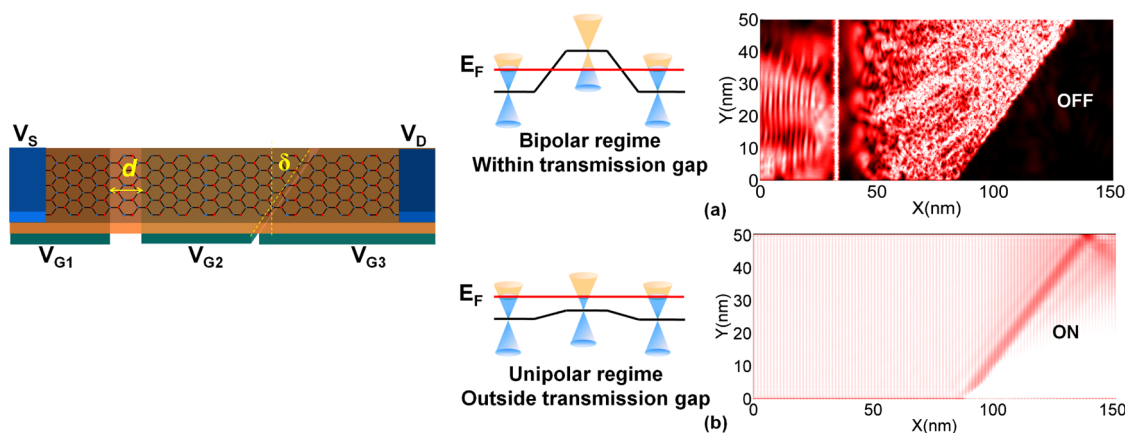
**Figure 4. Electron confinement in the proposed GPNJ device.** Schematic of collimator−barrier pair that sequentially filters all propagating modes is shown on left. Numerical current density plot from NEGF showing (a) blocking of carrier flow in the bipolar npn OFF state, (b) unipolar nn⁻n ON state, current flowing from source to drain. White (black) areas indicate high (low) local current density.

two ways to turn ON the device—by getting rid of both junctions (Figure 1c, biasing scheme 1: vary $V_{G2}$ for npn → nnn) or only one junction (Figure 1d, biasing scheme 2: vary $V_{G3}$ for npn → npp). Earlier we showed the transfer curve $I_D–V_G$ (Figure 1c) as a function of $V_{G2}$. Changing $V_{G2}$ compromises the collimation action of the first junction, and the condition of the transmission gap becomes the bipolarity (eq 5). Therefore, the effective conduction band moves by the same amount as the applied gate voltage, yielding $\sim KT$ln10 mV/dec change in current. In Figure 1d, $V_{G3}$ is changed and a drastically different transfer characteristic emerges. For simplicity, we keep the first junction split gated but with no tilt. The first junction limits transmission primarily around normal incidence ($\theta \approx 0$), while the second junction, tilted at $\delta$, increases the effective angle of incidence by the gate tilt angle $\delta$.[24] All the electrons are then reflected if the critical angle of the second junction is less than $\delta$

$$\theta_C = \sin^{-1}\left|\frac{n_R}{n_L}\right| < \delta \qquad (9)$$

where $n_R$ and $n_L$ are doping concentrations on the two sides of junction 2. The resulting transmission vanishes over a range of energies (following from eq 9), which can be expressed as[20]

$$E_G = V_0 \frac{2\sin\delta}{\cos^2\delta} \qquad (10)$$

analogous to ref 20, despite being a different (simpler) geometry, with the tilt angle $\delta$ replacing the barrier angle $\theta_B$. Such tunability of the transmission gap for an abrupt junction bears a direct impact on the subthreshold slope. Once we enter the unipolar regime for the second junction (pn to pp), the critical angle from Snell's law (discussed earlier) comes into play and the effective band edge shifts by $-qV_{G3}/(1 - \sin \delta)$ at the thin oxide limit. That means the transmission gap overlaps with the

Fermi distribution at a higher rate than usual with change in gate bias, leading to a subthermal slope, $SS = \alpha KT\text{ln}10(1 - \sin \delta)$[20] steeper than the Landauer limit, where $\alpha$ is inversely proportional to the filtering strength $(k_F d)^{1/2}$ of the first junction. However, since the first junction is always present under this scheme, it will reduce the ON current and the ON−OFF ratio by a factor of $(k_F d)^{1/2}$,[25] compared to eqs 7 and 8.

**Numerical Simulation of Quantum Flow.** To demonstrate carrier trajectories in the proposed device, we numerically simulate the device (150 nm × 50 nm) using the non-equilibrium Green's function formalism (NEGF) (see Methods). Figure 4a,b shows the local current density. The source and drain Fermi levels are at $\mu_S = 0$ and $\mu_D = -qV_{DS}$. To visualize the current distribution in the device at the Fermi level, we apply a small drain bias $V_{DS}$ so that all electrons are at same quasi-Fermi level (as indicated by the red line in Figure 4). The nn⁻n ON state (Figure 4b) shows current from source to drain, while the npn OFF state (Figure 4a) shows very little current inside the final wedge connected to the drain. Most of the electrons that do not cross the tilted junction are redirected toward the source. Some electrons, especially the secondary modes ($\theta > 0$), are rejected by the initial collimator after edge reflections and tend to build up in the central wedge. The buildup of carriers increases the local quasi-Fermi level $\mu$ until the injection rate at the left junction, set by the transmission rate in eq 2, equals the leakage rate at the right tilted junction. The leakage is given by the exponentially reduced transmission in eq 4 plus additional edge-scattering-based pathways (a model was presented in ref 24 including an edge reflection parameter $\eta$) and direct tunneling through the central region depending upon its length. To minimize the effect of specular edge scattering, further modeling is needed to redirect electrons towards the source, through better gate design, or by possible blocking of incoming electrons

through Coulomb repulsion from the electrons piling up in the central region.

## CONCLUSION

In summary, by manipulating the angle-dependent chiral tunneling of GPNJ with the physical parameters of the gates, we can controllably suppress Klein tunneling and create a transmission gap, as opposed to a structural band gap. This is accomplished by combining the angular filtering at a split junction with the experimentally demonstrated[23] chiral tunneling across tilted junctions, such that the transmission lobes across multiple junctions become orthogonal to each other in the OFF state. The ON state simply requires biasing either one or both junctions to the unipolar regime making the ON current close to that of pristine graphene. Furthermore, by choosing a suitable biasing scheme, the transmission gap becomes highly gate tunable, yielding a subthermal turn ON that beats the Landauer switching limit. We consider such transport characteristics as a viable solution for the lack of band gap in graphene and suitable for low power beyond CMOS applications.

## METHODS

**Extracting $T_{av}$ from Transport Measurement.** In the experiment,[23] the junction resistance was extracted from

$$Rj_{expt} = [R(V_{G1}, V_{G2}) + R(V_{G2}, V_{G1}) - R(V_{G1}, V_{G1}) - R(V_{G2}, V_{G2})]/2 \quad (11)$$

The above equation eliminates contact and device resistance due to scatterings and leaves out the resistance contribution from the pn junction only. Theoretically, the total resistance $R_{Total} = 1/G$ can be divided into two parts (contact and device resistance). From eq 1

$$R_{Total} = [G_0]^{-1} \frac{1}{MT_{av}} \quad (12)$$

$$= [G_0]^{-1} \left[ \frac{1}{M} + \frac{1 - T_{av}}{MT_{av}} \right] \quad (13)$$

In the presence of a pn junction with nonunity $T_{av}$, the second term can be considered as the junction resistance

$$Rj = [G_0]^{-1} \left[ \frac{1 - T_{av}}{MT_{av}} \right] \quad (14)$$

The theoretical $T_{av}$ is already known (Supporting Information eq S2). The experimental $T_{av}$ can be found by plugging the value of $Rj_{expt}$ from measurement in eq 14. The only unknown value remains is the number of modes, $M = (W/\pi)(\Delta E(V_G)/\hbar v_F)$, where $\Delta E = \hbar v_F (\pi C_G V_G/q)^{1/2}$ is the shift of Dirac point with gate voltage $V_G$. The gate capacitance is calculated from a simple parallel plate capacitor model $C_G = \varepsilon/t_{ox}$ where gate oxide thickness $t_{ox}$ is 100 nm.

**NEGF Simulation.** The central quantity is the retarded Green's function

$$\mathscr{G} = (EI - H - U - \Sigma_1 - \Sigma_2)^{-1} \quad (15)$$

$H$ is the Hamiltonian matrix of graphene, described here with a minimal one $p_z$ orbital basis per carbon atom with $t_0 = -3$ eV being the hopping parameter. $\Sigma_{1,2}$ are the self-energy matrices for the semi-infinite source and drain leads, assumed to be extensions of the graphene sheet, and $\Gamma_{1,2}$ are the corresponding anti-Hermitian parts representing the energy level broadening associated with charge injection and removal. $U$ is the device electrostatic potential. The current from $i$th atom to $j$th atom is calculated from[28]

$$I_{i,j} = \frac{2q}{h} \int dE \text{Im}[\mathscr{G}_{i,j}^n(E)H_{j,i} - H_{i,j}\mathscr{G}_{j,i}^n(E)] \quad (16)$$

electron correlation function, $\mathscr{G}^n = \mathscr{G}\Sigma^{in}\mathscr{G}^\dagger$ and in-scattering function, $\Sigma^{in} = \Gamma_S f_S + \Gamma_D f_D$. $I_{i,j}$ is nonzero only if the $i$th atom and $j$th atoms are neighbors. The total current at an atomic site can be found by adding all the components vectorially, $I_i = \sum_j \vec{I}_{i,j}$.[26] Recursive Green's function algorithm (RGFA) is employed to extract relevant blocks of $\mathscr{G}$ and $\mathscr{G}^n$.[29,30]

*Conflict of Interest:* The authors declare no competing financial interest.

*Supporting Information Available:* Definition of average transmission per mode and detail derivation of transmission gap. This material is available free of charge *via* the Internet at http://pubs.acs.org.

## REFERENCES AND NOTES

1. Castro Neto, A. H.; Guinea, F.; Peres, N. M. R.; Novoselov, K. S.; Geim, A. K. The Electronic Properties of Graphene. *Rev. Mod. Phys.* **2009**, *81*, 109–162.
2. Novoselov, K. S.; Geim, A. K.; Morozov, S. V.; Jiang, D.; Katsnelson, M. I.; Grigorieva, I. V.; Dubonos, S. V.; Firsov, A. A. Two-Dimensional Gas of Massless Dirac Fermions in Graphene. *Nature* **2005**, *438*, 197–200.
3. Zhang, Y.; Tan, Y.-W.; Stormer, H. L.; Kim, P. Experimental Observation of the Quantum Hall Effect and Berry's Phase in Graphene. *Nature* **2005**, *438*, 201–204.
4. Beenakker, C. W. J. Colloquium: Andreev Reflection and Klein Tunneling in Graphene. *Rev. Mod. Phys.* **2008**, *80*, 1337–1354.
5. Lin, Y.-M.; Jenkins, K. A.; Valdes-Garcia, A.; Small, J. P.; Farmer, D. B.; Avouris, P. Operation of Graphene Transistors at Gigahertz Frequencies. *Nano Lett.* **2009**, *9*, 422–426.
6. Balandin, A. A.; Ghosh, S.; Bao, W.; Calizo, I.; Teweldebrhan, D.; Miao, F.; Lau, C. N. Superior Thermal Conductivity of Single-Layer Graphene. *Nano Lett.* **2008**, *8*, 902–907.
7. Bunch, J. S.; Verbridge, S. S.; Alden, J. S.; van der Zande, A. M.; Parpia, J. M.; Craighead, H. G.; McEuen, P. L. Impermeable Atomic Membranes from Graphene Sheets. *Nano Lett.* **2008**, *8*, 2458–2462.
8. Lee, C.; Wei, X.; Kysar, J. W.; Hone, J. Measurement of the Elastic Properties and Intrinsic Strength of Monolayer Graphene. *Science* **2008**, *321*, 385–388.
9. Zhou, S. Y.; Gweon, G.-H.; Graf, J.; Fedrov, A. V.; Spataru, C. D.; Diehl, R. D.; Kopelevich, Y.; Lee, D. H.; Louie, S. G.; Lanzara, A. First Direct Observation of Dirac Fermions in Graphite. *Nature* **2006**, *2*, 595–599.
10. Cheianov, V. V.; Fal'ko, V.; Altshuler, B. L. The Focusing of Electron Flow and a Veselago Lens in Graphene p-n Junctions. *Science* **2007**, *315*, 1252–1255.
11. Cserti, J.; Pályi, A.; Péterfalvi, C. Caustics Due to a Negative Refractive Index in Circular Graphene p-n Junctions. *Phys. Rev. Lett.* **2007**, *99*, 246801.
12. Péterfalvi, C.; Pályi, A.; Cserti, J. Electron Flow in Circular n-p Junctions of Bilayer Graphene. *Phys. Rev. B* **2009**, *80*, 075416.
13. Bolotin, K.; Sikes, K.; Jiang, Z.; Klima, M.; Fudenberg, G.; Hone, J.; Kim, P.; Stormer, H. Ultrahigh Electron Mobility in Suspended Graphene. *Solid State Commun.* **2008**, *146*, 351–355.
14. Morozov, S. V.; Novoselov, K. S.; Katsnelson, M. I.; Schedin, F.; Elias, D. C.; Jaszczak, J. A.; Geim, A. K. Giant Intrinsic Carrier Mobilities in Graphene and Its Bilayer. *Phys. Rev. Lett.* **2008**, *100*, 016602.

15. Mecklenburg, M.; Regan, B. Spin and the Honeycomb Lattice: Lessons from Graphene. *Phys. Rev. Lett.* **2011**, *106*, 116803.

16. Unluer, D.; Tseng, F.; Ghosh, A. W.; Stan, M. R. Monolithically Patterned Wide— Narrow—Wide All-Graphene Devices. *IEEE Trans. Nanotechnol.* **2011**, *10*, 931–939.

17. Schwierz, F. Graphene Transistors. *Nat. Nanotechnol.* **2010**, *5*, 487–496.

18. Tseng, F.; Ghosh, A. W. From Low-Bias Mobility to High-Bias Current Saturation: Fundamental Trade-offs in Graphene Based Transistors. *arXiv1003.4551* **2010**.

19. Novoselov, K. S.; McCann, E.; Morozov, S. V.; Fal'ko, V. I.; Katsnelson, M. I.; Zeitler, U.; Jiang, D.; Schedin, F.; Geim, A. K. Unconventional Quantum Hall Effectand Berry's Phase of $2\pi$ in Bilayer Graphene. *Nat. Phys.* **2006**, *2*, 177–180.

20. Sajjad, R. N.; Ghosh, A. W. High Efficiency Switching Using Graphene Based Electron "Optics". *Appl. Phys. Lett.* **2011**, *99*, 123101.

21. Katsnelson, M. I.; Novoselov, K. S.; Geim, A. K. Chiral Tunnelling and the Klein Paradox in Graphene. *Nat. Phys.* **2006**, *2*, 620–625.

22. Young, A. F.; Kim, P. Quantum Interference and Klein Tunnelling in Graphene Heterojunctions. *Nat. Phys.* **2009**, *5*, 222–226.

23. Sutar, S.; Comfort, E. S.; Liu, J.; Taniguchi, T.; Watanabe, K.; Lee, J. U. Angle-Dependent Carrier Transmission in Graphene p-n Junctions. *Nano Lett.* **2012**, *12*, 4460–4464.

24. Sajjad, R. N.; Sutar, S.; Lee, J. U.; Ghosh, A. Manifestation of Chiral Tunneling at a Tilted Graphene pn Junction. *Phys. Rev. B* **2012**, *86*, 155412.

25. Cheianov, V. V.; Fal'ko, V. I. Selective Transmission of Dirac Electrons and Ballistic Magnetoresistance of n-p Junctions in Graphene. *Phys. Rev. B* **2006**, *74*, 041403.

26. Sajjad, R. N.; Polanco, C. A.; Ghosh, A. W. Atomistic Deconstruction of Current Flow in Graphene Based Heterojunctions. *J. Comput. Electron.* **2013**, *12*, 232–247.

27. Low, T.; Hong, S.; Appenzeller, J.; Datta, S.; Lundstrom, M. Conductance Asymmetry of Graphene p-n Junction. *IEEE Trans. Electron Devices* **2009**, *56*, 1292–1299.

28. Datta, S. *Electronic Transport in Mesoscopic Systems*; Cambridge University Press, Cambridge, UK, 1997.

29. Alam, K.; Lake, R. K. Leakage and Performance of Zero-Schottky-Barrier Carbon Nanotube Transistors. *J. Appl. Phys.* **2005**, *98*, 064307–064307.

30. Svizhenko, A.; Anantram, M. P.; Govindan, T. R.; Biegel, B.; Venugopal, R. Two-Dimensional Quantum Mechanical Modeling of Nanotransistors. *J. Appl. Phys.* **2002**, *91*, 2343–2354.